15th Triennial World Congress, Barcelona, Spain

PERFORMANCE OF JAPANESE ROBOTIC ARMS OF THE INTERNATIONAL SPACE STATION

Y. Wakabayashi*, H. Morimoto*, N. Satoh*,
M. Hayashi, Y. Aiko**, M. Suzuki[+]**

** National Space Development Agency of Japan*
*** NEC TOSHIBA Space Systems, Ltd.*
[+]Hitachi, Ltd.

Abstract: Two types of Japanese robot arms will be used for the Japanese Experiment Module of the International Space Station. Main Arm, the larger one, carries payloads installed on the exposed area. Small Fine Arm, the smaller one, is attached to the tip of Main Arm when it is used, and handles small-sized on-orbit payloads. Causes identified as aggravating factor of performance include backlash of gears, resonance of arms, and visual measurement error. The results of qualifying tests of these robotic arms show the validity of their design. This paper presents the performance of the robotic arms derived from the test results. *Copyright © 2002 IFAC*

Keywords: Robot arms, Robotic manipulators, Space robotics, Performance characteristics, Fault tolerant systems, Force control

1. INTRODUCTION

The Japanese Experiment Module (JEM) of the International Space Station (ISS) has two types of robotic arms. Main Arm (MA), the larger one, is a six degree-of-freedom arm of about ten meters in length and 780 kg in weight. It has an endeffector at the end of the arm, a common device that other robotic arms in ISS use for grappling objects. MA carries payloads installed on the exposed area by holding another common interface in ISS, Grapple Fixture. Small Fine Arm (SFA), the smaller one, is also a six degree-of-freedom arm of about two meters in length and 190 kg in weight. A Grapple Fixture is attached on the bottom of SFA so that MA can hold SFA when used. At the end of SFA it has a JEM-unique endeffector called Tool. Small-sized payloads have Tool Fixtures that mate with Tool in order to be handled. For space robotic arms seizing objects securely is one of the most significant issues. Failure could mean producing space debris, collision with other space modules, loss of crucial equipment, and so on. Thus berthing task needs to be most guaranteed. The pair of MA and SFA is called JEM Remote Manipulator System (JEMRMS). The tasks of JEMRMS are described in section 2. In section 3 performance of the JEMRMS' elements is presented. Section 4 shows the performance of JEMRMS as a system. The results of qualifying test that proves the validity of the design of the robotic arms are presented in section 5.

2. ROBOT ARM TASKS

2.1 Main Arm's tasks

MA handles with payloads weighing from 500 kg to 7000 kg. JEM has a unique area where space-exposed experiment is carried out by berthing box-shaped payloads that contain experiment equipments to both sides of a flat space-exposed area, the Exposed Facility (EF). This box-shaped standard payload weighs 500 kg and is 1m×1m×1.9m in size. MA is also able to carry a larger object including JEM's modules such as EF up to 7000 kg in weight. When MA berths a payload to the EF, it follows a unique path called L-shaped approach in order to avoid jamming with capture mechanism on EF. Figure 1 shows the path but the capture mechanism is not drawn to highlight the interface point.

2.2 Small Fine Arm's tasks

SFA is designed to handle small-sized payloads of the weight from 80 kg to 300 kg. Up to 80 kg SFA is able to use its force moment accommodation function. This function is useful when SFA needs to push the payload so that it can follow the contour of guide plates. SFA also has a wrench at the tip and is able to rotate a bolt head to apply torque to it. SFA is expected to support space experiment using its dexterous tool at the tip.

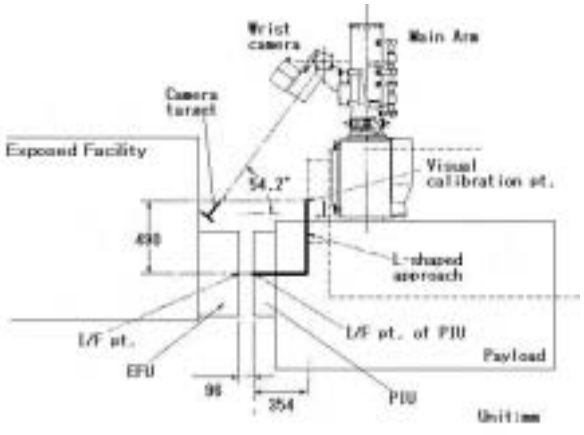

Fig. 1 L-shaped approach of MA

3. PERFORNANCE OF JEMRMS ELEMENTS

In this section the characteristics of the robot elements are described, and performance data that are crucial to mission tasks as a space manipulator are also presented.

3.1 Performance of Main Arm (MA)

1) MA Joint Mechanism;
MA has 6 identical revolving joints, each of which realizes ~400Nm output torque by a brushless DC-motor with solid lubricated gears (ratio =1400:1), controlled by a 16-bit dedicated DSP located in its joint electronics and a magnetic resolver (LSB = 0.002deg). It has a set of solid lubricated main bearing with constant preload. The joint module has an off-activated ceramic brake on its motor axis, and an additional optical absolute encoder (LSB = 0.006deg, Accuracy = 0.011deg) between inner/outer housings.
Backlash and Alignment uncertainties; The rotational uncertainty of "Backlash" and tilt angle uncertainty of "inner/outer housing alignment" are important factors for handling accuracy, because the arm tip position might be fluctuated within their range under zero-g environment in space. The rotational backlash was designed and measured to be 0.043~0.056deg, and housing alignment for bending within ~0.012deg for each joint. These are derived from mechanical designs, and valid in a wide operational temperature range. Figure 2 shows a typical backlash, in which hysteresis behavior up to ±10Nm external torque and drifting characteristics are observed.

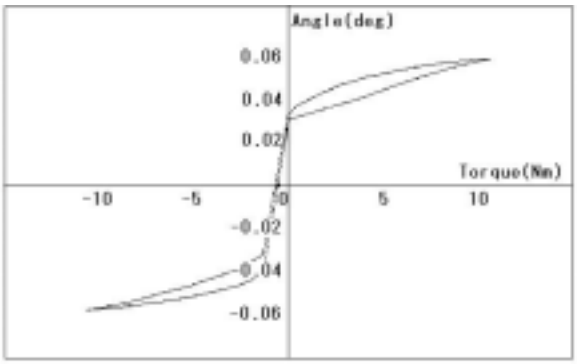

Fig. 2 MA Joint characteristics

Joint Stiffness MA-Joint stiffness is a major element of arm stiffness, because stiffness due to the two booms of CFRP is much larger than that of the joints. Rotational stiffness of each joint including that of housing was evaluated ~3 x 10^5 Nm/rad, and bending stiffness was ~1 x 10^6 Nm/rad.
Joint Back Drive Torque The tip of MA is able to be moved by applying external force/torque for payload mating/de-mating tasks. In this "Limp-mode", the external torque rotates each joint against the joint back-drive torque, which is mainly caused from gear's friction. Because of solid lubricant characteristics, the back-drive torque was evaluated to be 10.4~20.3 Nm in thermal vacuum test, while 17.5~39.0 Nm in N_2-gas environment.

Brakes; The brake torque ranges from 150 to 270 Nm.

2) Control system and its performance
The MA is controlled by dual 32-bit MPUs located in the pressurized module via dual MIL-STD-1553B networks. The control algorithm is based on the classical theory with phase lead/lag filters. Changing the control parameters allows the system to deal with a wide range of payload's weight. Angle open loop Bode plot of the joint-#1 in Fig.3 shows its stability and response.

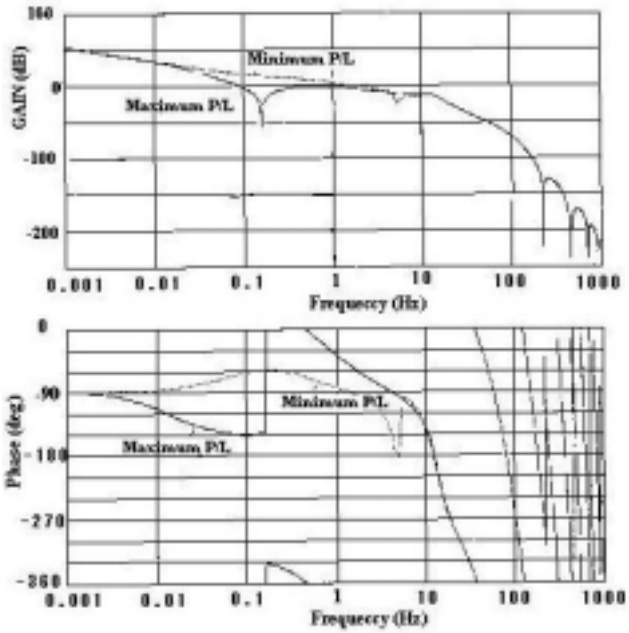

Fig. 3 Bode plot of MA Joint angle (open loop)

3) Visual Sensing System
Visual sensing using 3-dimensional 4-point target on the worksite is a primary basis for automatic manipulation. A wrist camera on the vicinity of the arm tip has pan/tilt and zoom/iris/focus capability for 6 degrees of freedom measurement. The pan/tilt capability allows MA to be positioned at the visual calibration point (the coarse positioning point) and at the interface point of Payload Interface Unit (PIU) (the fine positioning point) via "L-shaped approach "path in Fig.1, even when a large payload covers the sight ahead of the arm.

3.2 Performance of Small Fine ARM (SFA)

The characteristics of SFA elements are described in this section, and performance data that are crucial to mission tasks as a space manipulator are also presented.

1) SFA Joint Mechanism
SFA has two sets of three identical revolving joints ([θ1-θ3] / [θ4-θ6]; numbering from the base), each of which realizes ~ 41/18 Nm output torque by a brushless DC motor with solid lubricated Harmonic Drive (ratio = 130/120: 1). SFA electronics box located at the base of SFA controls angular velocity by five 32-bit MPUs using magnetic encoders (LSB =0.006 deg). The joint has a set of solid lubricated main bearings with constant preload, and has an off-activated ceramic brake on motor axis. Furthermore there is a force/torque sensor on its tip that enables compliance control and active-limp control.
Backlash and Alignment; The rotational backlash was evaluated 0.03~0.06deg, and housing alignment for bending 0.01~0.03 degree for each joint. Figure 4 shows SFA's joint characteristics including backlash.

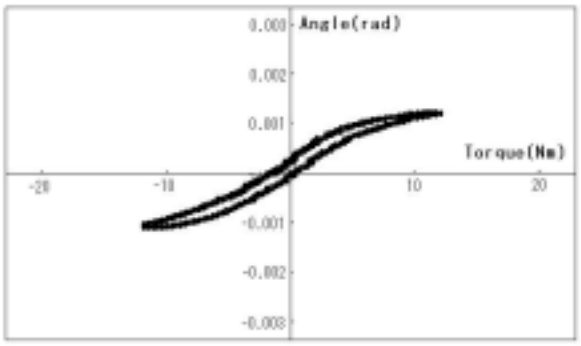

Fig. 4 SFA Joint characteristics

Joint Stiffness SFA-Joint stiffness is a major factor of arm stiffness, because stiffness due to the booms are much larger than that of the joints. Rotational stiffness of each joint is shown in Table 1. The stiffness is mainly due to the flexibility of Harmonic Drives excepting that of θ1, which is affected by housing flexibility.

Table 1Rotational Stiffness of SFA Joints (Nm/rad)

ƒÆP	ƒÆQ	ƒÆR	ƒÆS	ƒÆT	ƒÆU
0.8×10^4	1.6×10^4	1.5×10^4	1.2×10^4	0.8×10^4	1.0×10^4

Joint Back-Drive Torque; Back-drive torque is less important for SFA than for MA, because SFA is actively limped using force/torque sensor for contact operations. SFA's back-drive torque was evaluated to be within ~10/8 Nm (in N_2-gas environment) excluding ~10Nm-max harness loss torque in orbital condition.
Brakes; The brake torque ranges from 40 to 120 Nm.

2) Force/Torque Sensor (FTS)
The FTS, made of aluminium alloy block, has accuracy of ~1N (<10N), ~2N (<60N) (LSB ~0.17N) within 60N full-range in force, and has accuracy of ~0.1Nm(<1Nm), ~0.3Nm (<10Nm)(LSB ~0.015Nm) within 9Nm full-range in momentum, even after overload force/momentum tests. Figure 5 shows a typical performance of the sensor when forces were measured after overload force test. Its cross-talk between force and torque will be tested soon.

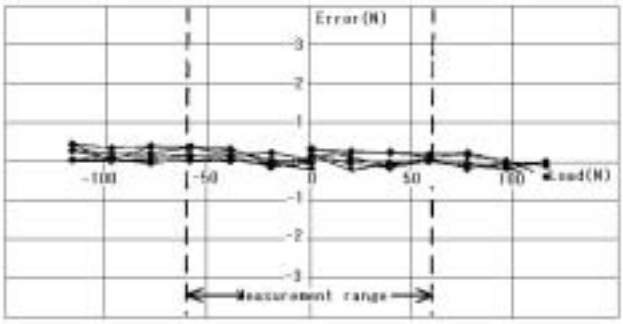

Fig. 5 SFA Force/Torque Sensor Performance (Force)

3) Control system and its performance
The SFA is also controlled by dual 32-bit MPUs in the pressurized module via dual MIL-STD-1553B. The control algorithm is based on the classical theory with a phase lead/lag filter. Changing the control parameters allows the system to deal with a wide range of payload's weight. Fig.6 shows open loop Bode plot of motor velocity of θ1 showing its stability and performance.

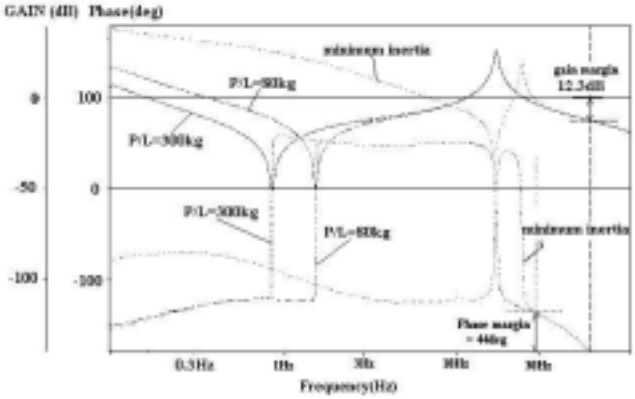

Fig. 6 Bode plot of SFA motor velocity (open loop)

4) Visual Sensing System
There is a fixed-focus camera on the wrist for visual sensing. A crewmember in the Pressurized Module normally operates SFA using joysticks in manual mode with a help of overlay templates superimposed on the display.

4. PERFORMANCE OF JEMRMS SYSTEM

Positioning error, deviation from nominal path, and stopping distance in emergency are presented as system performance in this section. This includes the case in which SFA is attached to servo-locked MA as well as individual MA/SFA, because SFA is always used in that configuration. For the purpose of system performance evaluations, we compared analysis (worst case) with system test data obtained using an air bearing floor in 2-dimentional arm movement.

The description of the movement is given in Table 2, and 3.

Table 2 Example movement for MA

Arm tip position / attitude [x,y,z,roll,pitch,yaw] (m,m,m,deg,deg,deg)	Arm tip velocity	Payload
[6.5,-0.5,-0.5,0,-90,0] ↓ [6.5,-0.5,0.5,0,-90,0]	10 mm/s	600 kg

Table 3 Example movement for SFA

Arm tip position/attitude [x,y,z,roll,pitch,yaw] (m,m,m,deg,deg,deg)	Arm tip velocity	Payload
[0.836,-0.18,0.365,0,0,0] ↓ [0.736,-0.18,0.365,0,0,0]	50 mm/s	80 kg

4-1. Positioning error

Table 4 shows what the contents of positioning error are. These are calculated by solving kinematics for each joint's performance.

Table 4 Positioning errors of MA (analysis)

	dx (mm)	dz (mm)	$d\theta_Y$
A1 backlash	<20.904	<20.904	<0.204
A2 Alignment	<16.370	<16.370	<0.199
A3 Assemble	<16.250	<16.250	<0.196
A4 Control error	<5.280	<5.280	<0.046
A5 Thermal	<2.200	<2.200	<0.028
A6 Total	<44.669	<44.669	<0.463

Total = A1 + $[A2, A3, A4, A5]_{RSS}$ where $[\cdot]_{RSS}$ denotes to take root sum square of elements in the bracket. Table 5 shows test results of positioning errors.

Table 5 Positioning errors of MA (test data)

	dx (mm)	dz (mm)	$d\theta_Y$ (deg)
B1 motor axis	2.2	6.9	0.07
B2 output axis	15.2	30.9	0.37
B3 3-D measurement	22.9	54.0	0.71

B1 means positioning error obtained by calculating forward kinematics on motor axis encoder data, so is B2 on output axis encoder data. B3 is evaluation by three-dimensional measuring equipment. Thus, B1 corresponds to A4, and B2 to (A4 + A1). B3 is equivalent to A6. These results show the validity of our analysis. Table 6 is final estimations of positioning performance in space, which is calculated by eliminating friction force of ground test.

Table 6 Onboard positioning errors of MA (estimation)

	dx (mm)	dz (mm)	$d\theta_Y$ (deg)
C1 motor axis	1.2	2.3	0.024
C2 output axis	14.7	29.2	0.370

As for SFA, Table 7 presents test data of positioning/attitude error of SFA and SFA on servo-locked MA.

Table 7 positioning/attitude error of SFA and SFA on servo-locked MA.

	Positioning error	Attitude error
SFA (SFA coordinate system)	<2.62 mm	<0.69 deg
SFA on servo-locked MA (MA coordinate system)	<8.28 mm	–

4-2. Deviation from nominal path

In the following tables, test data and analysis are shown.

Table 8 Deviation from nominal path of MA (MA coordinate system)

	Along path	Radial
Test data	50.9 mm	16.4 mm
Analysis	52.1 mm	14.3 mm

Table 9 Deviation from nominal path of SFA (SFA coordinate system)

	Along path	Radial
Analysis	26.2 mm	6.3 mm

Note that test data is reflected on analysis. Distance to move is extended from 10 cm to 40 cm to realize maximum velocity 50 mm/s in this analysis only.

4-3. Emergency stop distance.

The following table shows safety performance of MA. The emergency stop distances in two different cases are shown. The test was conducted on the ground, and its test data is taken into account to on-orbit analysis in which friction force is eliminated.

Table 10 Emergency stop distances (test and on-orbit analysis)

	Translation		Rotational	
	Test	analysis	Test	analysis
Payload: 600 kg Tip speed: 60 mm/s	117.0 mm	129.6 mm	0.39 deg	0.77 deg
Payload: 3000 kg Tip speed: 30 mm/s	89.5 mm	121.6 mm	0.51 deg	0.87 deg

5. MISSION EVALUATION

As stated in section 2, there are many berthing tasks for the robot arms. We present in this section a task of a Standard Payload (PL) berthing to an Exposed Facility Unit (EFU) on the EF by MA as an example to show the validity of the robot system. As an example we choose #7 EFU of the twelve EFUs on the EF. The two quantities evaluated in sub-sections 5-1 and 5-2 are used in order to examine if MA satisfies berthing conditions. The berthing conditions are given in sub-section 5-3, and each condition is examined and summarized in table 13 in the sub-section.

5-1 Deviation from nominal paths

Because influences from gravity and friction force between ground support equipment and the flat test plate in the ground test are not negligible, an offline simulator is used to evaluate deviation of the tip position of MA from the nominal paths. At each moment two types of quantities are specified to define the deviation: deviation along the nominal path direction and radial deviation from the nominal path. The maximum of these quantities along the nominal path are taken as deviation on the nominal path. The result of the simulation for a typical example of movement in the direction of arm-tip z-axis is as follows.

Table 11 Deviation from nominal paths (arm-tip coordinate system)

	Along path	Radial	$d\theta_x$	$d\theta_y$	$d\theta_z$
deviation	20.0 mm	8.2 mm	0.005 deg	0.189 deg	0.003 deg

Note that the following errors are not included in the above results because of the nature of the offline simulator. Thus, these errors are added in sub-section 5-2.

・Thermal distortion
・Grapple error of the endeffector
・Visual positioning error

5-2 Positioning accuracy

By summing up the following errors considering statistic characteristics of each element, the total positioning error of the interface point of PIU of PL grappled by MA can be estimated. If this point is inside the capture envelope of the capture mechanism, the berthing will be achieved.

Statistic property of each error is represented by type U, B, and R. U: uniform, B: bias, R: random. The total translation error consists of two types of translation errors; one is pure translation, and the other is translation due to attitude error. The latter one is estimated as multiplication of the length of the lever from Grapple Fixture of PL to Payload Interface Unit (PIU) by attitude error of each type. For example, translation due to attitude error of type B is defined as:

Translation due to attitude error of type B = [attitude errors of B]$_{RSS} \times$ L, where $[\cdot]_{RSS}$ means to take root sum square of elements in the bracket, and L is a length from Grapple Fixture of PL to PIU of the PL.

Visual calibration; The wrist camera of MA sees a 4-point visual target near the capture mechanism to calibrate MA's tip position and its attitude with respect to the visual target. When an image of the target appears on the crew operator's screen, the crew operator adjusts 4 cursors on the screen so that they overlap the 4 points of the target, which completes the visual calibration. Visual calibration includes many error sources and it is the dominant cause of total positioning error. The result of the total positioning errors is presented using EFU coordinate system in Table 12. EFU coordinate system is defined in Fig. 7 in which PIU and EFU are illustrated.

5-3 Berthing conditions and their examination

Table 13 shows the berthing conditions and summarizes their examination.

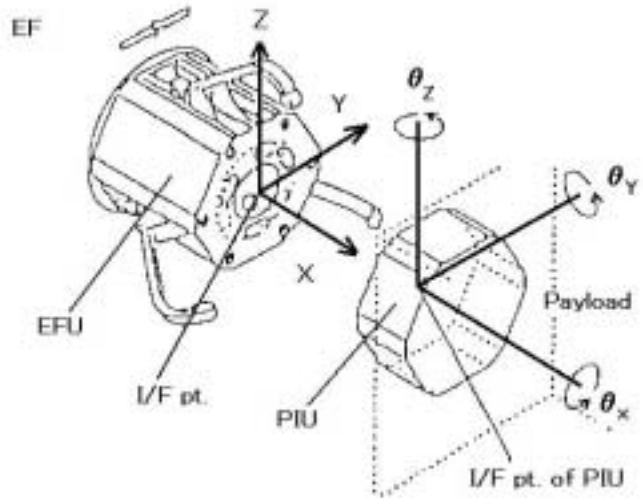

Fig. 7 PIU approaching EFU
EFU coordinate system shown

Table 12 Total positioning error of Payload at EFU#7 (EFU coordinate system)

	Translation error (mm)				Attitude error (deg)			
	dx	dy	dz	$(dy^2+dz^2)^{1/2}$	$d\theta_x$	$d\theta_Y$	$d\theta_Z$	$(d\theta_Y^2+ d\theta_Z^2)^{1/2}$
Positioning	-10.3	-28.0	-24.0	36.9	±0.6	±0.80	±1.1	±1.4
	22.7	28.0	24.0					
Capture envelope	-18.0	−	−	88	±1.2	−	−	±1.6
	43.2	−	−			−	−	

Table 13 Berthing conditions and their examination

Items			Conditions	Evaluated/analysed values
Fine positioning conditions	Approach speed	Forward	$V_x \leqq 30$ mm/s	Set approach speed 10 mm/s
		radial	$(V_y^2+V_z^2)^{1/2} \leqq 30$ mm/s	
		rotational	$(\omega_x^2+\omega_y^2+\omega_z^2)^{1/2} \leqq 0.5$ deg/s	
	Effective mass of MA's wrist		$M_{eff} \leqq 400$ kg	320 kg
	Approach envelope	Envelope	Specific envelope	55.5 mm
		Attitude	$(\theta_x^2+\theta_y^2+\theta_z^2)^{1/2} \leqq 3$ deg	1.7 deg
	Capture conditions	Envelope	Specific envelope	See Table 12
		Wobble	$(\theta_y^2+\theta_z^2)^{1/2} \leqq 1.6$ deg	Less than 1.4 deg
		Axial	$\theta_x \leqq 1.2$ deg	Less than 0.6 deg
Mate/demate conditions Between EF-payload	Back drive force of arm	Axial	$F_x \leqq 110$ N	43 N
		Radial	$(F_y^2+F_z^2)^{1/2} \leqq 110$ N	72 N
	Back drive torque of arm	rotational	$T_x \leqq 220$ Nm	179 Nm
		Wobble	$(T_y^2+T_z^2)^{1/2} \leqq 220$ Nm	196 Nm
Mate/demate conditions between payload-arm	Back drive force of arm	Axial	$F_x \leqq 110$ N	43 N
		Radial	$(F_y^2+F_z^2)^{1/2} \leqq 110$ N	72 N
	Back drive torque of arm	rotational	$T_x \leqq 220$ Nm	179 Nm
		Wobble	$(T_y^2+T_z^2)^{1/2} \leqq 220$ Nm	196 Nm

CONCLUSIONS

The performance of the JEM manipulator system was described showing its elemental data, system test data and analysis. It was confirmed that berthing tasks, one of most important mission tasks of JEM manipulator would be successfully performed on orbit.

Acronym

JEM	Japanese Experiment Module
JEMRMS	JEM Remote Manipulator System
MA	Main Arm
SFA	Small Fine Arm
EF	Exposed Facility
EFU	Exposed Facility Unit
PIU	Payload Interface Unit

REFERENCES

M. Nagatomo et al.,(1998).
Results of the On-Orbit Manipulator Flight Demonstration (MFD). In: *Proceedings of the twenty-first international symposium on space technology and science*, Volume I, 622-627. ISTS, JAPAN

T. Kasai et al., (1999).
Results of the ETS-7 mission –Rendezvous docking and space robotics experiments. In: *Fifth International Symposium on Artificial Intelligence Robotics and Automation in Space*, 299-306. ESA, the Netherlands.

T. Matsueda et al., (1999).
Safety approach of Japanese Space Manipulator System. In: *Fifth International Symposium on Artificial Intelligence Robotics and Automation in Space*, 531-537. ESA, the Netherlands.

S. Doi, Y.Wakabayashi, et al.,(2001)
Control Aspect of Japanese Experimental Module Remote Manipulator System, In: *IFAC Conference on Telematics Applications in Automation and Robotics,* 473-478, GMA, Germany

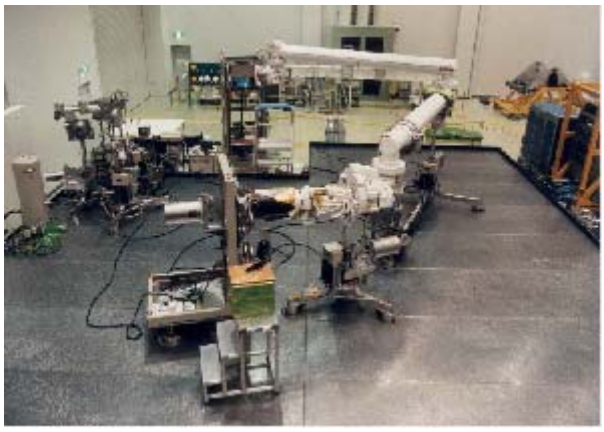

Fig. 7 Main Arm in the ground test (Flight model)